Precipitation of supersaturated solute in H ion irradiated Fe-Au and Fe-Au-W alloys studied by positron annihilation spectroscopy

Zhang, Z.; Zhang, S.; Yao, Z.; Tao, X.; Cao, X.; Zhang, P.; Kuang, P.; Fu, Y.; van Dijk, N. H.; van der Zwaag, S.

DOI
10.1016/j.nimb.2021.06.022

Publication date
2021

Document Version
Final published version

Published in
Nuclear Instruments and Methods in Physics Research, Section B: Beam Interactions with Materials and Atoms

Citation (APA)
Zhang, Z., Zhang, S., Yao, Z., Tao, X., Cao, X., Zhang, P., Kuang, P., Fu, Y., van Dijk, N. H., & van der Zwaag, S. (2021). Precipitation of supersaturated solute in H ion irradiated Fe-Au and Fe-Au-W alloys studied by positron annihilation spectroscopy. *Nuclear Instruments and Methods in Physics Research, Section B: Beam Interactions with Materials and Atoms*, *505*, 50-57. https://doi.org/10.1016/j.nimb.2021.06.022

Nuclear Instruments and Methods in Physics Research B 505 (2021) 50–57

Contents lists available at ScienceDirect

Nuclear Inst. and Methods in Physics Research, B

journal homepage: www.elsevier.com/locate/nimb

Precipitation of supersaturated solute in H ion irradiated Fe-Au and Fe-Au-W alloys studied by positron annihilation spectroscopy

Z. Zhang [a,d], S. Zhang [a,b,*], Z. Yao [a,b], X. Tao [c], X. Cao [d,*], P. Zhang [d], P. Kuang [d], Y. Fu [e,f], N. H. van Dijk [e], S. van der Zwaag [f]

[a] College of Materials and Technology, Nanjing University of Aeronautics and Astronautics, Nanjing 211106, PR China
[b] Key Laboratory of Materials Preparation and Protection for Harsh Environment (Nanjing University of Aeronautics and Astronautics), Ministry of Industry and Information Technology, Nanjing 211106, PR China
[c] School of Materials Science and Engineering, Nanjing Institute of Technology, Nanjing 211167, PR China
[d] Institute of High Energy Physics, Chinese Academy of Sciences, Beijing 100049, PR China
[e] Fundamental Aspects of Materials and Energygroup, Faculty of Applied Sciences, Delft University of Technology, Mekelweg 15, 2629 JB Delft, the Netherlands
[f] Novel Aerospace Materials Group, Faculty of Aerospace Engineering, Delft University of Technology, Delft, the Netherlands

ARTICLE INFO

Keywords:
Precipitation
Hydrogen ion irradiation
Thermal aging
Positron annihilation spectroscopy
Fe-based alloys

ABSTRACT

The effect of thermal aging of homogenized Fe-Au and Fe-Au-W alloys, irradiated at room temperature with hydrogen ions, was studied for an aging treatment at 300 °C for aging times up to 100 h. The aging behavior of the Fe-based alloys is compared to the results for pure Fe. The precipitation behavior of Au-rich and W-rich precipitates and its correlation to the H^+ irradiation-induced defects is investigated by variable energy positron annihilation spectroscopy (VEPAS). The formation of open-volume defects after irradiation is monitored by an increase in the *S* parameter, while the recovery of the vacancy-like defects and the formation of precipitates are signalled by an increase in the *W* parameter. Au-rich precipitation continuously develops during long-term aging, as indicated by the increase in the *W* parameter. The change of the W parameter in the Fe-Au-W alloy is not only due to the effect of solute W on the Au precipitates, but also because of the interface of W-rich Laves phase with matrix.

1. Introduction

The ferrous components of the reactors are unavoidably exposed to neutron radiation, which leads to severe displacements of the atoms and high H/He concentrations, in the form of vacancies, dislocation, voids and H/He bubbles [1–3]. This microstructural damage ultimately causes swelling, irradiation hardening and embrittlement, which induces undesirable material degradation that reduces the service lifetime and stability of nuclear materials [4–6]. The microstructural mechanisms of these property deteriorations are ascribed to the effect that transmutation H/He would interact with the intrinsic and irradiation open-volume defects in which they are trapped [7]. Therefore, it is important to study the interaction between the H/He interstitials with open-volume defects, leading to the formation of gas-vacancy complexes [8]. At the same time, dislocations in the metal will trap helium atoms to form the helium-dislocation complexes (He_nD), and this in turn will affect the formation of He_nV_m [9,10]. Hydrogen atoms, as the smallest interstitial atoms, are easily trapped by a vacancy, which enhances the activity of the vacancy and promotes the formation of vacancy clusters. This can be attributed to the low thermal stability and recovery of hydrogen-vacancy complexes (H_nV_m) [11]. The de-trapping energy of hydrogen atoms is only 1 eV [12], and the decomposition of H_nV_m complexes readily occurs during the heat treatment, which results in the release of hydrogen from the vacancies and the formation of new open volume.

Many studies have found that alloying elements can interact with irradiation defects and affect their evolution. Lu et al. reported on the irradiation enhanced Cr segregation at the grain boundary in various ferritic/martensitic alloys [13]. In the high Cr austenitic stainless steel, the segregated Cr atoms interact with dislocation and irradiation-induced precipitation $Cr_{23}C_6$ takes place in the dislocation loops while the Cr segregation on the helium bubble surface retards the mobility of the helium bubbles formed [14].In the Fe-Cu model alloys, thermally activated Cu precipitation takes place at deformation-induced open-

* Corresponding authors at: College of Materials and Technology, Nanjing University of Aeronautics and Astronautics, Nanjing 211106, PR China (S. Zhang).
E-mail addresses: zhangsha2003@aliyun.com (S. Zhang), caoxzh@ihep.ac.cn (X. Cao).

https://doi.org/10.1016/j.nimb.2021.06.022
Received 2 March 2021; Received in revised form 23 May 2021; Accepted 7 June 2021
Available online 8 September 2021
0168-583X/

volume defects, especially dislocations [15]. Zhang et al. substituted the healing element Cu by Au, and reported that Au atoms prefer to segregate to dislocations and this creates a favorable interaction between Au precipitates and grain boundary creep cavities formed during creep loading of Fe-Au alloys [16]. A similar effect was noted for supersaturated solute W atoms which also diffuse to the cavity and precipitate in the form of Laves phase particles on the free cavity surface and hence fill the cavity [17]. For the open-volume defects caused by irradiation, similar to the deformation-induced defects, solute segregation and redistribution results in swelling reduction, which is attributed to the trapping of open-volume defects by solute elements. This dependence is proven by the strong spatial correlation between the irradiation-induced defects and precipitates formed. This was nicely shown for a Fe-Cu alloy in which all other radiation mitigation effects were excluded by selecting a high purity Fe-Cu alloy. In Monte Carlo simulations, the attraction of substitutional He and Cu is stronger than for Cu-V complexes, which indicates that He can promote the precipitation of Cu in iron [18]. Experimentally, the formation of Cu-V complexes and vacancy-like defects surrounded by tiny Cu precipitates in Fe-Cu model alloys was detected by slow positron spectroscopy. In the previous study of hydrogen irradiated metal, also an effect of the alloying elements on the irradiated-induced defects was observed [19,20]. Also recent work on the hydrogen implanted C-containing FeMnNiCoCr high-entropy alloys demonstrated that the interaction between the interstitial C atoms and irradiated-induced vacancies will inhibit the aggregation of vacancy clusters [19]. A study on the hydrogen trapping sites in ferritic steels indicated that the origin of the trapping sites is not the assumed misfit dislocations between the vanadium carbides (VC) precipitate and matrix, but the carbon vacancy of the V_4C_3 precipitates [21].

Previous studies have demonstrated [22,23] that there exists an even stronger spatial correlation of Au precipitates with He and Fe ion irradiation-induced defects than in the case of irradiated Fe-Cu alloys *Ab initio* calculations indicated that the binding energy of Au-V_n is stronger than that of Cu-V_n, and that He atoms can weaken the trapping capability of vacancies. In our previous study, it was shown that radiation hardening of Fe-Au alloy barely took place when increasing the irradiation dose because of Au precipitation on irradiation-induced defects [22]. The previous studies focused on high purity binary alloys in which only one healing mechanism was assumed to take place, but real steels are multi-component systems so it is interesting to explore the healing reactions in more complex alloys containing several alloying elements each capable to induced a corrective reaction on irradiation induced damage. Rather than going directly to multi-component steels in which the individual reactions cannot be separated it is interesting to consider ternary alloys in which the number of reactions can be foreseen and analysed properly. The ternary alloy Fe-Au-W seems an ideal candidate as the response of Au to irradiation damage is well documented and W is a well-known alloying element in nuclear reactor steels demonstrating good solution strengthening and reduced neutron activation. A recent study on the same Fe-Au-W alloy as to be used in the present study nicely showed the competitive precipitation reactions of both alloying elements when exposed to high temperatures [24].

In the present study, the effect of Au addition and the combined of Au and W addition on irradiation defects is investigated using variable energy positron annihilation spectroscopy (VEPAS) to unravel the interaction between solute Au and W atoms and irradiation defects during the subsequent aging treatment.

2. Experimental

The Fe-Au and Fe-Au-W model alloys were prepared by vacuum arc melting (pure Fe as a controlled group) followed by casting, hot rolling leading to 1 mm thick foils. The as-received Fe-Au-W alloy contains 1.22 at.% W and 0.916 at.% Au with balance Fe and the as-received Fe-Au alloy contains 1.23 at.% Au with balance Fe. Both alloys were solution treated in evacuated and sealed quartz tube filled with ultrahigh-purity argon gas at 868 °C for 5 h, and subsequently quenched into water at room temperature. The pure iron sample was fully annealed at 750 °C in vacuum (about 10^{-5} Pa). The specimens were first mechanically polished with grade 800–2000 silicon carbide paper and chemo-mechanically polished using a suspension of colloidal silica (0.04 μm) to mirror-like surface and remove stress in the top layer. The specimens were irradiated on the 320 kV-platform at the Institute of Modern Physics, Chinese Academy of Science (CAS). Irradiations were performed using 120 keV H^+ ions to fluences of 2.7×10^{17} ions/cm^2 at room temperature. Then variable energy positron annihilation spectroscopy (VEPAS) measurements were carried out on all the samples after aging treatment from 0.5 to 100 h at a temperature of 300 °C.

The VEPAS measurements were carried out on a magnetically guided slow positron beam with ^{22}Na radiation source (activity of 1.85 GBq). The energy of the positrons in the beam was varied from 0.5 to 25 keV. The probed depth of the slow positrons is defined by their incident energy and is calculated by the following empirical equation [25,26],

$$Z(E) = \left(\frac{40}{\rho}\right)E^{1.6} \quad (1)$$

where *Z(E)* is the depth below surface in nm, *E* is the incident energy of the slow positrons in keV and ρ is the density of the material in g/cm^3. Doppler broadening of the annihilation photon peak was measured using a high-purity Ge detector with an energy resolution of 1.1 keV at the 511 keV peak. Two parameters (*S* and *W*) were calculated from the annihilation photo-peak. The *S* and *W* parameters were defined as the ratio of counts in the central energy region (511 ± 0.75 keV) and in two wings regions (515.0–519.2 keV and 502.8–507.0 keV), respectively. The information of annihilation mechanism of positrons with low/high-momentum electrons in material can be directly reflected by the value of the *S/W* parameter, respectively. Doppler broadening spectroscopy was carried out to characterize the homogenized Fe-Au and Fe-Au-W alloys before and after irradiation and after aging times up to 100 h of aging. For comparison complementary spectra for pure Fe were measured. Coincidence Doppler broadening (CDB) spectra were carried out to measure the homogenized Fe-Au/Fe-Au-W alloys (unirradiated) and irradiated pure Fe, Fe-Au, Fe-Au-W having received aging treatment at 300 °C up to 100 h using two-Ge-detectors, which decreased the background for the high momentum contributions and was useful in studying the variation in Au content around the defect site [27].

According to the two-state capture model, the *S* and *W* parameter were denoted by the following formulation [28]:

$$S = (1-f) \times S_b + f \times S_d \quad (2)$$

$$W = (1-f) \times W_b + f \times W_d \quad (3)$$

In that, the *S* parameters of defect trapping state and free state are S_b and S_d, and the *W* parameters of defect trapping state and free state are W_b and W_d. Then there is $S = R\times(W\text{-}W_b) + S_b$, in which $R=(S_d\text{-}S_b)/(W_d\text{-}W_b)$, called as the gradient of *S-W* curve, is independent of the size or concentration of vacancy-like defects. Since the *S* parameter reflects the annihilation with low momentum electrons, and the *W* reflects the annihilation with high momentum electrons, the competition of annihilation result in the increase in *S* with the decrease in *W*.

3. Results and discussion

3.1. SRIM simulation

Irradiated by 120 keV H^+ ions, the displacement per atom (dpa) and He concentration profiles as a function of depth are calculated using the Stopping and Range of Ions in Matter (SRIM) computer program [27,29–33]. The calculation is based on the Kinchin-Pease mode and the displacement energy of Fe is set to be 40 eV [29,31,32]. Because of low content of solute elements, the simulation data for the pure Fe is also

representative for both Fe-based alloys. As shown in Fig. 1, for a fluence of 2.7×10^{17} ions/cm^2, the irradiation-induced damage in the Fe-based materials reaches a maximum value of approximately 0.5 dpa at a depth of 530 nm. The implanted H ions extend from surface to the depth of about 800 nm and the peak in hydrogen concentration reaches a value of 20 at.%, located at approximately a depth of 560 nm. And positron stopping profiles of 15 keV had been added in Fig. 1 [33].

The positrons are a sensitive probe for vacancy-type defects in the Fe-based materials. The trapping behavior of positron at precipitate is a common feature, because positron will always be captured by near defects, like vacancy, dislocation. Moreover, positrons are trapped by different embedded particles, like Cu clusters/precipitates [34] or Au precipitates [35]. The *S* parameter represents the fraction of positron annihilations as a result of the interaction with low-momentum electrons and increases for an increasing fraction of open volume defects. The *W* parameter reflects the fraction of positron annihilations with high-momentum electrons. The calculated positron affinities of Fe, Au and W atoms are −3.84, −4.59 and −1.31 eV [36], respectively. Since the positron affinity of Au is by 0.75 eV lower than that of Fe, while the positron affinity of W is higher than that of Fe, we can conclude that Au-rich clusters (precipitates or solute–vacancy complexes) are regarded as preferential potential sinks for the positrons, whereas the positrons are not sensitive to the W-rich clusters. The annihilation of positrons at Au-rich precipitates will cause the *W* parameters to increase by positron annihilation of high-momentum electrons.

3.2. Doppler broadening spectroscopy

The *S* and *W* parameters as function of incident positron energy (*S-E* and *W-E* curves) are compared between the three Fe-based materials (Fe, Fe-Au, Fe-Au-W) for unirradiated and irradiated samples and irradiated samples with subsequent aging for different aging times. As shown in Fig. 2, for the unirradiated samples no significant differences are observed for the three materials, while for all three materials the *S* parameter (Fig. 2(a)–(c)) is clearly enhanced due to irradiation. The increase in the *S* parameter corresponds to the formation and growth of vacancy-like defects in the irradiated alloys [37]. The *S* parameter for irradiated pure Fe is much higher than that of the irradiated Fe-Au and Fe-Au-W alloys, which indicates that the addition of Au inhibits the formation of vacancy-like defects. Little difference is observed between the irradiated Fe-Au and Fe-Au-W alloys.

In the irradiated samples, hydrogen atoms (H_n) would be trapped and occupy vacancies (V_m) to form the hydrogen-vacancy complexes (H_nV_m) at room temperature, which can affect the annihilation of positrons with the electrons in vacancy-like defects. After irradiation, the

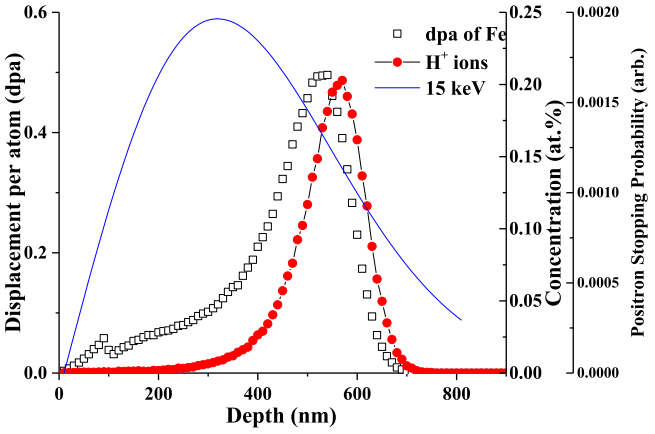

Fig. 1. Radiation damage in Fe-based samples for a fluence of 2.7×10^{17} ions/cm^2 in units of displacement per atom (dpa) and the corresponding hydrogen concentration depth profile obtained from SRIM calculations, and depth profile of positron stopping probability for positron energy of 15 keV in Fe.

300 °C aging treatment has been carried out for aging times ranging from 0.5 to 100 h for all three samples. During the aging treatment, the evolution of the *S* parameter with aging time shows pronounced differences for the three materials. For pure Fe, a peak in the *S* parameter as a function of positron energy is already present after 0.5 h of aging, as shown in Fig. 2(a). With increasing aging times, the peak in the *S* parameter became less pronounced until it vanished after 100 h of aging, which indicated that the H_nV_m complexes were decomposed [7,37–39]. A large amount of hydrogen atoms migrated and escaped from the vacancies, while the remaining vacancy-like defects still caused an increase of the *S* parameter with respect to the unirradiated sample. In Fig. 2(b), which shows the data for the Fe-Au material, the peak in the *S* parameter as a function of positron energy for the Fe-Au alloy appears after 1 h aging treatment, and the peak in the S parameter disappears with increasing aging time, and the curve tends to become flat. This *S* parameter peak concluded the appearance of Au precipitates. The increase of *S* parameter was attributed to the misfit between the precipitates and the matrix, and the peak disappeared due to the growth of precipitates which decreased the S parameters and increased the *W* parameters [35]. During the initial aging step of 0.5 h, the H-V complexes begin to decompose to form new vacancies, leading to an increase in the *S* parameter, while the solute Au atoms occupy the vacancies, causing a reduction in the *S* parameter [34,38]. The new vacancies formed by decomposition of the H_nV_m clusters will lead to the increase of *S* parameter, and also the new vacancies partly occupied by thermally activated Au atoms and recovered duo to annealing will cause the decrease of *S* parameter. The decrease in the *S* parameter is greater than the increase, which results in a slight decrease in the overall *S* parameter. However, after 1 h of aging more H_nV_m complexes decompose, and the vacancies migrate and aggregate to form clusters, leading to the development of the *S* parameter peak.

For the Fe-Au-W alloy, the *S* parameter as a function of positron energy reached a weak peak directly after irradiation. The *S* parameter then gradually decreased with aging time without the presence of a peak. Through first principle calculations it is found that the vacancies are more likely to be formed on the W side of the Fe/W interface then on the Fe side [40]. This kind of H_nV_m complexes decompose, which does not lead to a large increase in the *S* parameter as observed for the H_nV_m decomposition in pure Fe. This is due to the lower positron affinity of W atom, i.e. the positrons are not easily annihilated with low-momentum electrons, which explained the absence of a peak for the Fe-Au-W alloy during the aging treatment. However, For the Fe-Au-W alloys, the Fe_2W Laves phase precipitates have hexagonal lattice structure with an high misfit in the bcc iron lattice [41]. The incoherent misfit of the Laves phases will become the trapping site for the positron [22], which caused the increase in the *S* parameter. Meanwhile, the synergistic self-healing effect of the Au/W elements on the irradiation defects in Fe-Au-W is greater than that of the Fe-Au alloy, and the decrease in the *S* parameter caused by this is greater than the increase in the *S* parameter caused by the incoherent effect of Laves phase. The combined reactions leads to the *S* parameter of the Fe-Au-W alloy being slightly lower than that of the Fe-Au alloys exposed to the same aging treatment.

The *W* parameter for pure Fe samples (Fig. 2(d)) demonstrates an obvious decrease due to irradiation. In contrast, a slight decrease in W parameter is observed for the irradiated Fe-Au and Fe-Au-W alloys (Fig. 2(e)–(f)). Since the *S* and *W* parameters are the result of a competition of annihilation in different states, the decrease in the *W* parameter primarily arises from the increase in the S parameter [37]. During irradiation at room temperature, little solute segregation and precipitation occurred. The subsequent aging treatment at 300 °C accelerates the continuous segregation and precipitation of Au and W. For the Fe-Au alloy, the Au atoms, just like the impurity H atoms, could occupy the vacancies, to form solute–vacancy complexes. The Au-V complexes would enhance the increase in *W* parameter. For the Fe-Au-W alloys, there is a phenomenon that the W parameters are lower than that of Fe-Au after 100 h long term aging treatment, which is

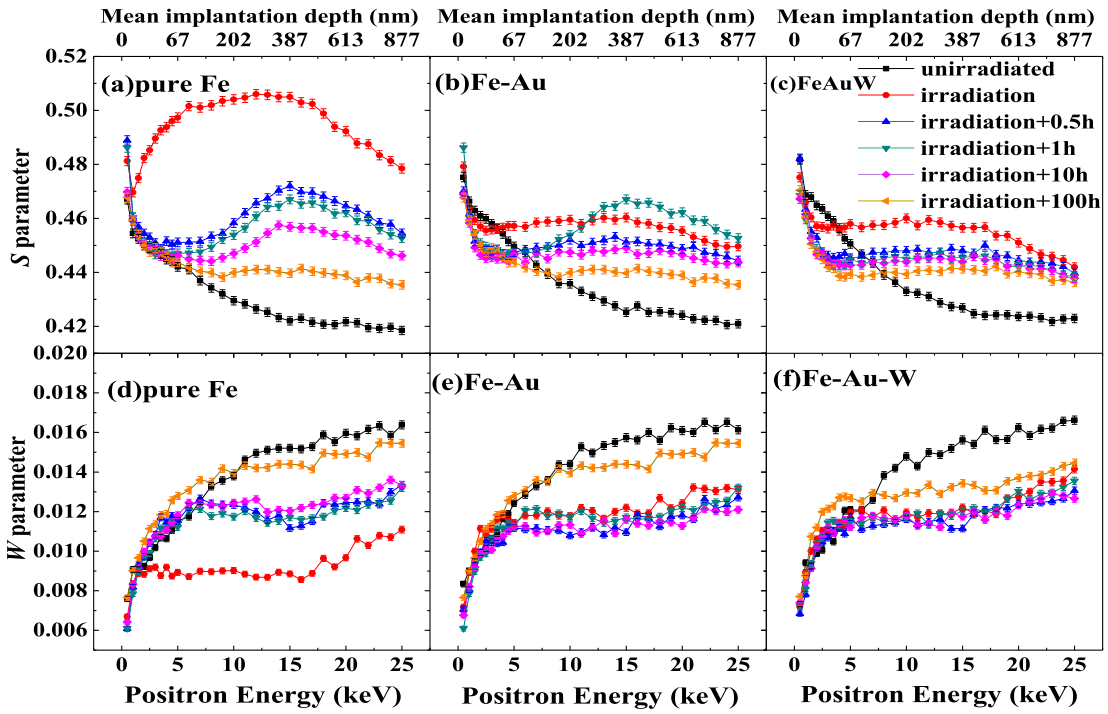

Fig. 2. Dependence of (a-c) *S-E* curves and (d-f) *W-E* curves on irradiation and aging time for pure Fe, the Fe–Au alloy and the Fe-Au-W alloy. For comparison, the *S-E* and *W-E* curves for the unirradiated samples are included.

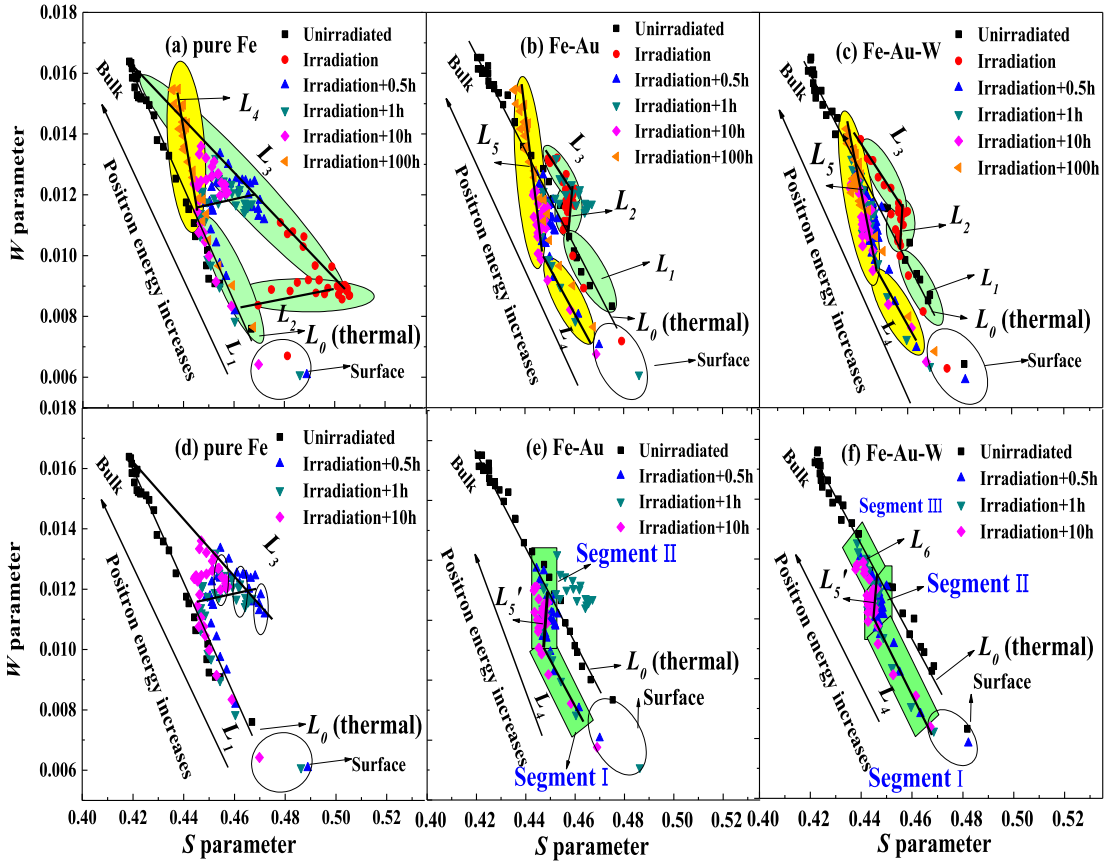

Fig. 3. *S-W* plots for (a) pure Fe, (b) Fe-Au alloy and (c) Fe-Au-W alloy samples for different conditions: unirradiated, irradiated and irradiated with aging different indicated aging times; (d) - (f) are part of *S-W* plots for the short term aged samples in (a), (b), (c).

attributed to two reasons. On one hand, the positrons trapped by misfit will not contribute to the *W* parameter. On the other hand, The W atoms encounter vacancy defects during the diffusion, which influence the surrounding chemical environment of the Au-V complex and hinder the aggregation of Au-V complexes.

The *S*-*W* plots reflect the correlation between the evolution of irradiation-induced defects and the generation of clusters or precipitates during aging. As shown in Fig. 3, for all the unirradiated samples the (*S, W*) points follow a single linear relationship (labelled as L_0): the *S* parameter decreases and the *W* parameter increases with increasing positron energy. The slopes of curves are similar for all three materials, which indicated that positrons were annihilated predominantly in the vicinity of Fe atoms (the unirradiated samples are homogenized materials). The difference in the electron densities caused by specific defects and chemical environment of precipitates lead to a difference in positron annihilation mechanisms, which corresponds to a difference in the evolution of the (*S*, *W*) couples. The *S*-*W* plots for the irradiated and subsequent aging samples cannot be described by a single straight line, indicating the change in local chemical environment of the positron annihilation site induced by the H^+ radiation or solute precipitates formed during aging.

For pure Fe the irradiated samples and irradiated samples with subsequent aging as shown Fig. 3(a), the (*S, W*) curves can be divided into three regions with labelled L_1, L_2, L_3, L_4, respectively. Close to the surface, the slope of line L_1 is the same as that of the unirradiated sample, indicating that the positrons are predominantly annihilated with Fe electrons. For an increasing positron implantation depth, the implanted H ions diffuse into the matrix and are likely to be trapped by vacancies, creating H_nV_m complexes. The positron annihilation with H electrons results in the change in slope of line L_2 for irradiated pure Fe, after 100 h of aging treatment, the *S*-*W* curve is obviously different from the samples at shorter aging times. Since the vacancy-type defects and irradiation dislocation loops coexist in the irradiated sample, the H_nV_m complexes have mostly decomposed after the long-term aging, causing the vacancies near the interstitial dislocation loops to migrate and recover [42], which results in more positron annihilations with dislocation loops instead of vacancies, vacancy complexes or clusters. Therefore, for short-term aging the *S*-*W* curve does not reflect the existence of dislocations, but is dominated by positron annihilations with the H_nV_m complexes.

The (*S,W*) evolution of the irradiated Fe-Au and Fe-Au-W alloys is significantly different from that of irradiated pure Fe. Because of the higher irradiation resistance of the Fe-Au alloy compared to irradiated pure Fe, the slope of L_2 for irradiated Fe-Au and irradiated pure Fe is notably different. The slight increase in the *S* parameter due to the lower concentration of defects and the obvious increase in the *W* parameter are due to the influence of the Au atoms on the chemical environment of the positron annihilation site. The deviation of slope of L_2 from that of L_0 is mainly due to the interaction between the solute Au atoms with vacancies. In contrast with the irradiated Fe-Au alloy, the (*S*, *W*) points in the line L_3 of the irradiated Fe-Au-W alloy are distributed over a wider range, as a result of the W atoms in the Fe-Au-W alloy.

Since the (*S, W*) points for the three materials are relatively dense In Fig. 3(a)–(c), the *S*-*W* curves for the shorter aging times of 0.5, 1 and 10 h are represented separately in Fig. 3(d)–(f). For irradiated pure Fe, through subsequent aging treatment, the recovery of vacancies by annealing results in a decrease in the *S* parameter and an increase in *W* parameter due to the competitive annihilation. This causes the (*S*, *W*) aggregated points to move to the deep bulk region. It is clear that the *S*-*W* plots for the irradiated short-time aging for the Fe-Au and Fe-Au-W alloys can be divided into two and three segments, respectively. In segment I, the lines L_4 are parallel for both unirradiated alloys, which demonstrated that the trapped positrons were still mainly annihilated with the Fe electrons. This indicates that the vacancy clusters in this segment, i.e. $Au_nV_m(n < m)$ complexes, are the dominant in the microstructure. As mentioned in the previous analysis of the *S*-*E* and *W*-*E* curves, because the H_nV_m complex decomposes and the Au-V complexes are gradually formed, the formation of Au_nV_m ($n < m$) results a situation where the vacancy clusters are dominant in the microstructure. At the same time, the changed chemical environment resulting from the decomposition of H_nV_m complexes is also reflected in the *S*-*W* plots for the irradiated Fe-Au alloy after 1 h of aging. Moreover, the irradiation-induced dislocation loops will also cause the trapped positrons to annihilate mainly with Fe electrons. In segment II, because of the thermally activated solute Au migration, more Au atoms decorated the open-volume defects [22,43], with the result that $Au_nV_m(n > m)$ complexes are the dominant defect type. It is noteworthy that for the Fe-Au-W alloy the part of L_6 curve in segment III is almost consistent with L_0, which suggests that the chemical environment around the vacancies decorated with Au atoms changes as a result of the presence of W atoms. With increasing aging time (100 h), the aggregation of Au-V complexes to form solute (Au) cluster or precipitates on the open-volume defect surface, leading to the shrinkage of vacancy clusters [24]. The original irradiation dislocation played an important role in site selectivity of precipitates. When the samples are exposed to high temperature for a long time, the Au-V complexes aggregate around the irradiated dislocations, which act as nucleation sites to form the Au-rich precipitates [23,44]. Therefore, Au precipitates and dislocations loops dominate the microstructure along the L_5 line [45]. For the Fe-Au-W alloy, simultaneously the mixtureof dislocations between the Au precipitates [23,45] and the Fe matrix act as nucleation sites of the W-rich Laves precipitates, which influence the precipitation behavior of Au-rich precipitates.

The *S* and *W* parameters for the irradiated and aged samples were normalized to those of their respective unirradiated samples with the purpose of enlarging specific information related to the nature of the vacancy-like defects and precipitates. The normalized *S* and *W* parameters were denoted by the following formulations [37]:

$$Snor = \Delta S/S = Nor\frac{Sirradiatedaged - Sunirradiated}{Sunirradiated} \tag{4}$$

$$WNor = \Delta W/W = \frac{Wirradiated(aged - Wirradiated)}{Wirradiated} \tag{5}$$

Fig. 4 indicates the dependence of $\Delta S/S(S_{Nor})$ and $\Delta W/W$ (W_{Nor}) parameters on the positron energy (implantation depth) in pure Fe and in the two Fe-based alloys directly after irradiation and after irradiation with subsequent aging. In Fig. 4(a), (b) and (c) it is found that the maximum value in $\Delta S/S$is reached at a depth about 387 nm (~15 keV) which is smaller than the damage peak depth (530 nm) in SRIM simulation. Through previous research [46], it is well known that the migration of vacancy defects in Fe already occurs around 200 K (below the room temperature). Because the samples are irradiated at RT and exposed at 300°Cin the aging treatment, the vacancy-like defects introduced by H^+ irradiation can easily migrate and diffuse to the surface region, which results in a shift of the peak position compared to the SRIM results [47]. The values of $\Delta S/S$ were negative from 1 to 5 keV. In the range of 1–5 keV, the S_{NOR} parameter of unirradiated samples was higher than the bulk values due to the effect of the surface region [48]. From the surface to the damage region, the S_{Nor} parameter gradually increases for all samples and reaches a peak due to the high H^+ ion energy and vacancy migration. On the contrary, the *S* parameters of all samples approach the bulk value in the deep region where the implantation positron energy is large. This implies that the irradiation-induced vacancy-like defects and solute precipitates influence the positron diffusion length. In the range from the irradiation damage region to the bulk the S_{Nor} parameter decreases with increasing aging time, which can be ascribed to the recovery of irradiation defects.

For the pure Fe, the W_{Nor} parameter decreases due to irradiation, which is ascribed that the predominant annihilation with irradiation-induced vacancy-like defects. Then, with increasing aging time at 300 °C, the recovery of vacancies and the decomposition of vacancy clusters leads to a decrease in the annihilation events with low-

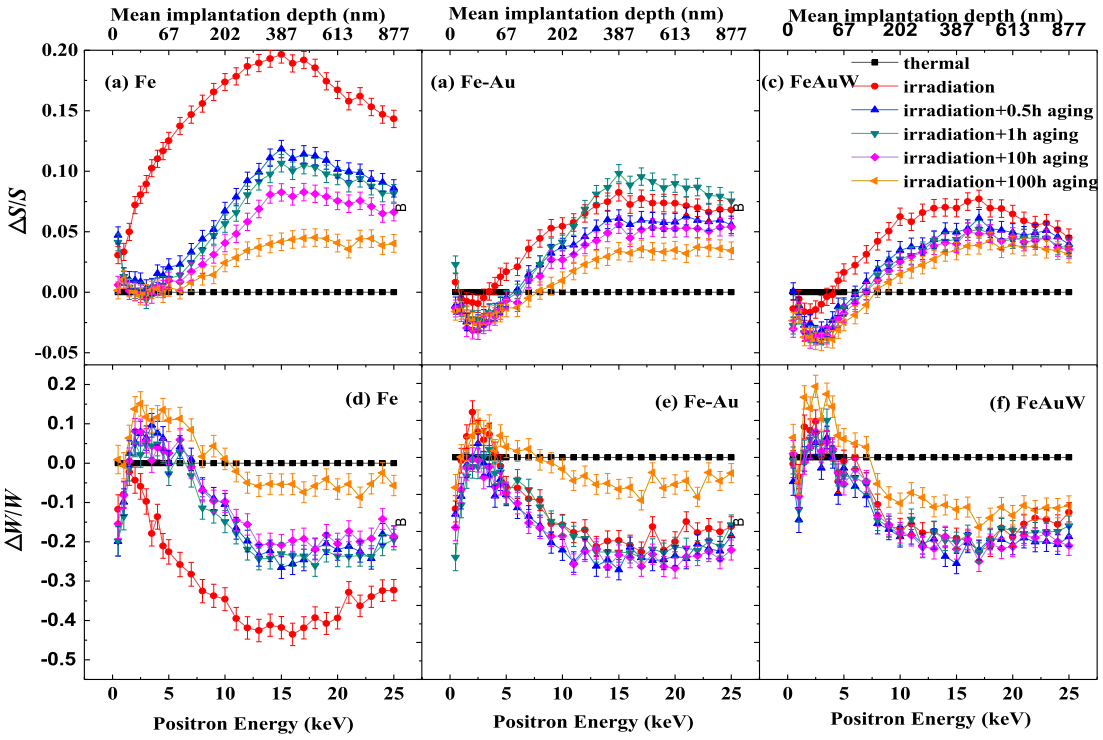

Fig. 4. $\Delta S/S$ and $\Delta W/W$as a function of the positron energy (depth) for irradiation and aging for 0.5, 1, 10 and 100 h in pure Fe, the Fe-Au alloy and the Fe-Au-W alloy.

momentum electrons, which causes an increase in W_{Nor}.

However, for the Fe-based alloys, the S_{Nor} and W_{Nor} parameters are lower than that of the irradiated sample at the beginning of the aging treatment (0.5 h) as a result of the start of recovery of vacancies and H atom desorption. In the alloys the vacancies introduced by irradiation can easily migrate during the aging treatment at elevated temperature, while some of them can encounter solute Au and W atoms to form solute–vacancy complexes. The vacancy-like defects induced by irradiation can facilitate the Au atoms to aggregate, and these Au atoms could substitute Fe atoms in the first shell surrounding the vacancy-like defect because of the fact that Au has a lower surface energy than Fe [49]. After short-term aging (0.5–10 h), the S_{Nor} and W_{Nor} parameters did not

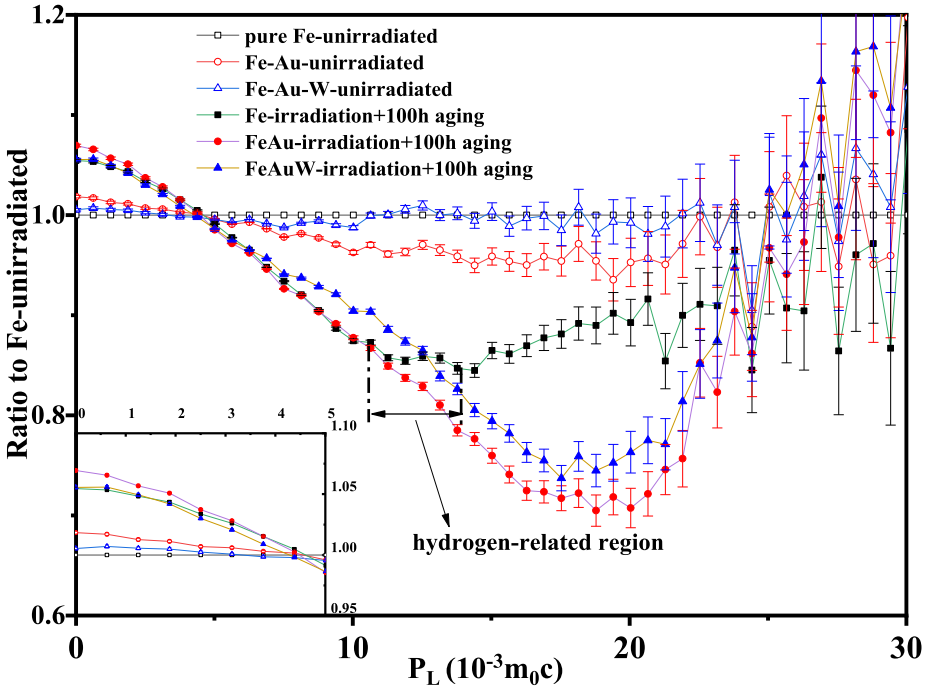

Fig. 5. Ratio curves of the CDB spectra of pure Fe, the Fe-Au alloy and the Fe-Au-W alloy in the homogenized (unirradiated) state and in the irradiated state after 100 h of aging. The ratio curves arewith respect to unirradiated pure Fe at a positron beam energy of 15 keV (387 nm). The inset shows the detailed information in the low-momentum region below $5 \times 10^{-3} m_0 c$ (the unit of momentum in which m_0 is the mass of electrons and c is the velocity of light).

change significantly, as a result of the coexistence of H atom desorption from open-volume defects and decoration of solute atoms. Furthermore, for the Fe-Au alloy, the increase in W_{Nor} for the irradiated samples after long aging (100 h) is due to an increase in the coverage of the open-volume defects by Au atoms. The increase for the Fe-Au-W alloy is not as large as that for the Fe-Au alloy, which is attributed to not only the influence of Fe_2W Laves phase precipitates on the precipitation behavior of Au but also the interface of W-rich Laves phase with matrix.

3.3. Coincidence Doppler broadening spectroscopy

Fig. 5 shows the evolution of the CDB ratio results for the homogenized materials in their unirradiated state and after irradiation followed by 100 h aging. The ratio curves are with respect to unirradiated pure Fe at positron beam energy of 15 keV. The ratio curves for the homogenized Fe-Au and Fe-Au-W alloys were are similar to the reference curve for pure Fe, indicating that solute atoms have been well dissolved in the matrix and the positrons are predominantly annihilated with Fe electrons. In the low-momentum region, no change was observed for the unirradiated samples. In contrast, the ratio of all the irradiated Fe-based samples has increased in the low momentum region ($<5 \times 10^{-3} m_0c$) due to the positron annihilation at the open volume defects induced by irradiation, as shown in the inset. The CDB ratio curves of the irradiated and aged Fe-Au and Fe-Au-W alloys show a broad valley at about $18 \times 10^{-3} m_0c$, which is characteristic for the *5d* electrons of Au clusters [35,50]. With the comparison between the three irradiated and aged samples, we can see the hydrogen-related region in the curve of irradiated pure Fe. Combined with some reports about helium-related region or similar hydrogen-related region, conclusion will be drawn [51–53]. If pure iron is irradiated with self-ions, there are so many vacancy-like defects inside interstitials. In this case, for the CDB curve with ratio to annealed pure Fe, the contribution of low momentum electrons annihilation will be increased and the curve flattens out gradually after a steep fall. Hydrogen is an isotope of deuterium which only has valance electrons, no core electrons. Therefore, the momentum distribution as detected in CDB measurements will be different [54]. However, H^+ ions irradiated iron contains a large amount of H-V complexes, which will directly change the annihilation probability of the localized positrons with Fe electrons. Therefore, the H_nV_m complexes resulted in the increase in the high momentum region, and the platform of hydrogen-related region occurs in this experiment besides other reports.

The characteristic valley of Au in the Fe–Au alloy is more pronounced than that of the Fe-Au-W alloy, indicating that the more Au atoms have decorated the open volume defects. Meanwhile, considering the incoherent or semi-coherent interface between precipitates and the matrix, the ratio curve of the Fe-Au alloy is slightly higher than that of Fe-Au-W alloy in the low-momentum region.

4. Summary and conclusion

Homogenized Fe-Au and Fe-Au-W model alloys, together with pure Fe, were irradiated with hydrogen ions at RT with a fluence of 2.7×10^{17} ions/cm^2. The irradiated samples were aged at 300 °C for aging times up to 100 h in order to investigate the correlation between thermally activated precipitation and irradiation-induced defects. VEPAS measurements were carried out to characterize both the defect and precipitate evolution after irradiation and subsequent aging. The *S* parameter for the Fe-based alloys is generally smaller compared to that for pure Fe, indicating a reduced irradiation swelling. For all irradiated samples aging at a temperature of 300 ℃ significantly reduces the *S* parameter. Au precipitation is found to be accelerated by long time aging, as indicated by the increase in *W* parameter. In the case of the ternary alloy the presence of W elements slows down the precipitation of Au at the defect sites. However, in the Fe-Au-W alloy, the increase in *W* parameter is not only affected by the effect of solute W on the Au precipitates, but also the interface of W-rich Laves phase with matrix.

CRediT authorship contribution statement

Z. Zhang: Conceptualization, Data curation, Writing - original draft. **S. Zhang:** Conceptualization, Project administration, Funding acquisition, Writing - review & editing. **Z. Yao:** Supervision, Funding acquisition. **X. Tao:** Data curation. **X. Cao:** Project administration, Funding acquisition. **P. Zhang:** Data curation. **P. Kuang:** Data curation. **Y. Fu:** Resources, Data curation. **N.H. Dijk:** Data curation, Writing - review & editing. **S. van der Zwaag:** Data curation, Writing - review & editing.

Declaration of Competing Interest

The authors declare that they have no known competing financial interests or personal relationships that could have appeared to influence the work reported in this paper.

Acknowledgments

The authors are grateful for the financial supports by the National Natural Science foundation of China (Grant No. 51701095); the Natural Science Foundation of Jiangsu Province, China (Grant No. BK20170798).Y. Fu acknowledges the financial support provided by China Scholarship Council (CSC).

References

[1] P.P. Liu, Q. Zhan, Z.Y. Fu, Y.P. Wei, Y.M. Wang, F.M. Wang, S. Ohnuki, F.R. Wan, Surface and internal microstructure damage of He-ion-irradiated CLAM steel studied by cross-sectional transmission electron microscopy, J. Alloy. Comp. 649 (2015) 859–864, https://doi.org/10.1016/j.jallcom.2015.07.177.
[2] P.J. Maziasz, Overview of microstructural evolution in neutron-irradiated austenitic stainless steels, J. Nucl. Mater. 205 (1993) 118–145, https://doi.org/10.1016/0022-3115(93)90077-C.
[3] S.J. Zinkle, P.J. Maziasz, R.E. Stoller, Dose dependence of the microstructural evolution in neutron-irradiated austenitic stainless steel, J. Nucl. Mater. 206 (1993) 266, https://doi.org/10.1016/0022-3115(93)90128-L.
[4] S.J. Zinkle, G.S. Was, Materials challenges in nuclear energy, Acta Mater. 61 (2013) 735–758, https://doi.org/10.1016/j.actamat.2012.11.004.
[5] T. Allen, J. Busby, M. Meyer, D. Petti, Materials challenges for nuclear systems, Mater. Today 13 (12) (2010) 14–23, https://doi.org/10.1016/S1369-7021(10)70220-0.
[6] V. Barabash, A. Peacock, S. Fabritsiev, G. Kalinin, S. Zinkle, A. Rowcliffe, J. W. Rensman, A.A. Tavassoli, P. Marmy, P.J. Karditsas, Materials challenges for ITER-current status and future activities, J. Nucl. Mater. 367 (2007) 21–32, https://doi.org/10.1016/j.jnucmat.2007.03.017.
[7] P. Zhang, S.X. Jin, E.Y. Lu, B.Y. Wang, Y.N. Zheng, D.Q. Yuan, X.Z. Cao, Effect of annealing on V_mH_n complexes in hydrogen ion irradiated Fe and Fe–0.3%Cu alloys, J. Nucl. Mater. 459 (2015) 301–305, https://doi.org/10.1016/j.jnucmat.2015.01.060.
[8] T. Zhu, X.Z. Cao, S.X. Jin, J.P. Wu, Y.H. Gong, E.Y. Lu, B.Y. Wang, R.S. Yu, L. Wei, Helium retention and thermal desorption from defects in Fe9Cr binary alloys, J. Nucl. Mater. 466 (2015) 522–525.
[9] Q. Xu, Y. Sugiura, X.Q. Pan, K. Sato, T. Yoshiie, Effects of dislocation-trapped helium on mechanical properties of Fe, Mat. Sci. Eng. A 612 (2014) 41–45.
[10] Y.H. Gong, X.Z. Cao, S.X. Jin, E.Y. Lu, Y.C. Hu, T. Zhu, P. Kuang, Q. Xu, B.Y. Wang, Effect of dislocations on helium retention in deformed pure iron, J. Nucl. Mater. 482 (2016) 93–98.
[11] T. Ishizaki, Q. Xu, T. Yoshiie, S. Nagata, T. Troev, The effect of hydrogen and helium on microvoid formation in iron and nickel, J. Nucl. Mater. 307 (2002) 961, https://doi.org/10.1016/S0022-3115(02)01279-5.
[12] T. Ishizaki, Q. Xu, T. Yoshiie, S. Nagata, The recovery of gas-vacancy-complexes in Fe Irradiated with High Energy H or He ions, Mater. Trans. 45 (2004) 9, https://doi.org/10.2320/matertrans.45.9.
[13] Z. Lu, R.G. Faulkner, G. Was, B.D. Wirth, Irradiation-induced grain boundary chromium microchemistry in high alloy ferritic steels, Scr. Mater. 58 (2002) 878, https://doi.org/10.1016/j.scriptamat.2008.01.004.
[14] S. Jin, L. Guo, F. Luo, Z. Yao, S. Ma, R. Tang, Ion irradiation-induced precipitation of $Cr_{23}C_6$ at dislocation loops in austenitic steel, Scr. Mater. 68 (2) (2013) 138–141, https://doi.org/10.1016/j.scriptamat.2012.10.002.
[15] S.M. He, N.H. van Dijk, H. Schut, E.R. Peekstok, S. van der Zwaag, Thermally activated precipitation at deformation-induced defects in Fe-Cu and Fe-Cu-B-N alloys studied by positron annihilation spectroscopy, Phys. Rev. B. 81 (2010), 094103, https://doi.org/10.1103/PhysRevB.81.094103.
[16] S. Zhang, C. Kwakernaak, F.D. Tichelaar, W.G. Sloof, M. Kuzmina, M. Herbig, D. Raabe, E. Brück, S. van der Zwaag, N.H. van Dijk, Autonomous Repair Mechanism of Creep Damage in Fe-Au and Fe-Au-B-N Alloys, Metall. Mater. Trans. A 46 (12) (2015) 5656–5670.

[17] H. Fang, N. Szymanski, C.D. Versteylen, P. Cloetens, C. Kwakernaak, W.G. Sloof, F. D. Tichelaar, S. Balachandran, M. Herbig, E. Brück, S. van der Zwaag, N.H. van Dijk, S.van der Zwaag, N.H.van Dijk, Self healing of creep damage in iron-based alloys by supersaturated tungsten, Acta Mater. 166 (2019) 531–542, https://doi.org/10.1016/j.actamat.2019.01.014.
[18] A.C. Arokiam, A.V. Barashev, D.J. Bacon, Y.N. Osetsky, Simulation of copper atom diffusion via the vacancy mechanism in a dilute Fe-Cu alloy, Phys. Rev. B 71 (2005) 174205, https://doi.org/10.1103/PhysRevB.71.174205.
[19] E.Y. Lu, I. Makkonen, K. Mizohata, Z.M. Li, F. Tuomisto, Effect of interstitial carbon on the evolution of early-stage irradiation damagein equi-atomic FeMnNiCoCr high-entropy alloys, J. Appl. Phys. 127 (2020) 025103, https://doi.org/10.1063/1.5130748.
[20] C. Hofer, E. Stergar, S.A. Maloy, Y.Q. Wang, P. Hosemann, An intermetallic forming steel under radiation for nuclear applications, J. Nucl. Mater. 458 (2015) 361–368.
[21] J. Takahashi, K. Kawakami, Y. Kobayashi, Y, Kobayashi, Origin of hydrogen trapping site in vanadium carbide precipitation strengthening steel, Acta Mater. 153 (2018) 193–204, https://doi.org/10.1016/j.actamat.2018.05.003.
[22] S. Zhang, J. Cizek, Z.J. Yao, M. Oleksandr, X.S. Kong, C.S. Liu, N. van Dijk, S. van der Zwaag, Self -healing of radiation-induced damage in Fe–Au and Fe–Cu alloys: Combining positron annihilation spectroscopy with TEM and ab initio calculations, J. Alloy. Compd. 817 (2020) 152765, https://doi.org/10.1016/j.jallcom.2019.152765.
[23] S.S. Zhang, Z.J. Yao, Z.K. Zhang, M. Oleksandr, F.D. Chen, X.Z. Cao, P. Zhang, Niels van Dijk, Sybrand van der Zwaag, Mediation of high temperature radiation damage in bcc iron by Au or Cuprecipitation, Nucl. Instrum. Meth. B 463 (2020) 69–75, https://doi.org/10.1016/j.nimb.2019.11.035.
[24] Y. Fu, C. Kwakernaak, W.G. Sloof, F.D. Tichelaar, E. Brück, S. van der Zwaag, N. H. van Dijk, Competitive Healing of Creep-Induced Damage in a Ternary Fe-3Au-4W Alloy, Metall. Mater. Trans. A 51 (2020) 4442–4455.
[25] J. Qiu, Y. Xin, X. Ju, L.P. Guo, B.Y. Wang, Y.R. Zhong, Q.Y. Huang, Y.C. Wu, Investigation by slow positron beam of defects in CLAM steel induced by helium and hydrogen implantation, Nucl. Instrum. Methods B 267 (18) (2009) 3162–3165, https://doi.org/10.1016/j.nimb.2009.06.045.
[26] H.P. Zhu, Z.G. Wang, X. Gao, M.H. Cui, B.S. Li, J.R. Sun, C.F. Yao, K.F. Wei, T. L. Shen, L.L. Pang, Y.B. Zhu, Y.F. Li, J. Wang, P. Song, P. Zhang, X.Z. Cao, Positron annihilation Doppler broadening spectroscopy study on Fe-ion irradiated NHS steel, Nucl. Instrum. Methods B 344 (2015) 5–10, https://doi.org/10.1016/j.nimb.2014.11.051.
[27] P. Asoka-Kumar, M. Alatalo, V.J. Ghosh, A.C. Kruseman, B. Nielsen, K.G. Lynn, Increased elemental specificity of positron annihilation spectra, Phys. Rev. Lett. 77 (10) (1996) 2097–2100, https://doi.org/10.1103/PhysRevLett.77.2097.
[28] T. Zhu, X. Cao, Research progress of hydrogen/helium effects in metal materials by positron annihilation spectroscopy, Acta Phys. Sin. 69 (2020) 177801.
[29] J.F. Ziegler, M.D. Ziegler, J.P. Biersack, SRIM-the stopping and range of ions in matter, Nucl. Instrum. Methods B. 268 (2010) 1818–1823, https://doi.org/10.1016/j.nimb.2010.02.091.
[30] J. Hunn, E. Lee, T. Byun, L. Mansur, Ion-irradiation-induced hardening in Inconel 718, J. Nucl. Mater. 296 (2001) 203–209, https://doi.org/10.1016/S0022-3115(01)00519-0.
[31] C.H.M. Broeders, A.Y. Konobeyev, Defect production efficiency in metals under neutron irradiation 328 (2004) 197–214, https://doi.org/10.1016/j.jnucmat.2004.05.002.
[32] R.E. Stoller, M.B. Toloczko, G.S. Was, A.G. Certain, S. Dwaraknath, F.A. Garner, On the use of SRIM for computing radiation damage exposure, Nucl. Instrum. Methods B 310 (2013) 75–80.
[33] V.J. Ghosh, G.C. Aers, Positron stopping in elemental systems: Monte Carlo calculations and scaling properties, Phys. Rev. 51 (1995) 45–49.
[34] S.X. Jin, X.Z. Cao, G.D. Cheng, X.Y. Lian, T. Zhu, P. Zhang, R.S. Yu, B.Y. Wang, Thermally promoted evolution of open-volume defects and Cu precipitates in the deformed FeCu alloys, J. Nucl. Mater. 501 (2018) 293–301, https://doi.org/10.1016/j.jnucmat.2018.01.061.
[35] S. Zhang, H. Schut, J. Čížek, F.D. Tichelaar, E. Brück, S. van der Zwaag, N.H. van Dijk, Positron annihilation study on deformation-induced Au precipitation in Fe–Au and Fe–Au–B–N alloys, J. Mater. Sci. 49 (6) (2014) 2509–2518.
[36] M.J. Puska, P. Lanki, R.M. Nieminen, Positron affinities for elemental metals, J. Phys. Condens. Matter. 1 (35) (1989) 6081–6094, https://doi.org/10.1088/0953-8984/1/35/008.
[37] S.X. Jin, P. Zhang, E.Y. Lu, L.P. Guo, B.Y. Wang, X.Z. Cao, Correlation between Cu precipitates and irradiation defects in Fe–Cu model alloys investigated by positron annihilation spectroscopy, Acta Mater. 103 (2016) 658–664, https://doi.org/10.1016/j.actamat.2015.10.051.
[38] T. Ishizaki, Q. Xu, T. Yoshiie, S. Nagata, The Recovery of Gas-Vacancy-Complexes in Fe Irradiated with High Energy H or He Ions 45 (2004) 9–12.
[39] K. Ono, M. Miyamoto, F. Kudo, Release of deuterium from irradiation damage in Fe–9Cr–2W ferritic alloy irradiated with deuterium ions, J. Nucl. Mater. 452 (1-3) (2014) 46–50, https://doi.org/10.1016/j.jnucmat.2014.04.043.
[40] J.M. Shi, N. Hashimoto, S. Isobe, J. Nucl. Sci. Technol. (2020), https://doi.org/10.1080/00223131.2020.1779143.
[41] Q. Li, Precipitation of Fe_2W Laves phase and modeling of its direct influence on the strength of a 12Cr-2W steel, Metall. Mater. Trans. A 37 (2006) 89.
[42] S.X. Jin, B. Mo, W.P. Zhang, T.M. Zhang, Y. Li, L.P. Guo, X.Z. Cao, B.Y. Wang, Towards understanding the evolution of dislocation loops and their interaction with vacancies in Fe9Cr alloy during the irradiation swelling incubation period, Materialia 5 (2019) 100241, https://doi.org/10.1016/j.mtla.2019.100241.
[43] Y. Nagai, Z. Tang, M. Hassegawa, T. Kanai, M. Saneyasu, Irradiation-induced Cu aggregations in Fe: An origin of embrittlement of reactor pressure vessel steels, Phys. Rev. B 63 (2001), 134110, https://doi.org/10.1103/PhysRevB.63.134110.
[44] E Hornbogen, The role of strain energy during precipitation of copper and gold from alpha iron, Acta Metall. 10 (5) (1962) 525–533, https://doi.org/10.1016/0001-6160(62)90197-9.
[45] S.X. Jin, X.Y. Lian, T. Zhu, Y.H. Gong, P. Zhang, X.Z. Cao, R.S. Yu, B.Y. Wang, Irradiation evolution of Cu precipitates in Fe1.0Cu alloy studied by positron annihilation spectroscopy, J. Nucl. Mater. 499 (2018) 65–70, https://doi.org/10.1016/j.jnucmat.2017.11.011.
[46] P. Hautojärvi, J. Johansson, A. Vehanen, J. Yli-Kauppila, P. Moser, Vacancy-carbon interaction in iron, Phys. Rev. Lett. 44 (20) (1980) 1326–1329, https://doi.org/10.1103/PhysRevLett.44.1326.
[47] Shuoxue Jin, Peng Zhang, Eryang Lu, Baoyi Wang, Daqing Yuan, Long Wei, Xingzhong Cao, Effect of annealing on Cu precipitates in H ion irradiated Fe-0.6% Cu studied by positron annihilation, J. Nucl. Mater. 479 (2016) 390–393, https://doi.org/10.1016/j.jnucmat.2016.07.039.
[48] S.X. Jin, X.Z. Cao, P. Zhang, E. Lu, L. Guo, R. Yu, B. Wang, Cu precipitates in hydrogen ion irradiated Fe–0.3%Cu alloy investigated by positron annihilation spectroscopy, JJAP Conf. Proc. 2 (2014), https://doi.org/10.7567/JJAPCP.2.011101.
[49] L. Vitos, A.V. Ruban, H.L. Skriver, J. Kollár, The surface energy of metals, Surf. Sci. 411 (1-2) (1998) 186–202, https://doi.org/10.1016/S0039-6028(98)00363-X.
[50] R.S. Brusa, W. Deng, G.P. Karwasz, A. Zecca, Doppler-broadening measurements of positron annihilation with high-momentum electrons in pure elements, Nucl. Instrum. Meth. B 194 (4) (2002) 519–531, https://doi.org/10.1016/S0168-583X(02)00953-9.
[51] V. Sabelová, V. Kršjak, J. Kuriplach, Y. Dai, V. Slugeň, Coincidence Doppler broadening study of Eurofer 97 irradiated in spallation environment, J. Nucl. Mater. 458 (2015) 350–354.
[52] Y. Liu, Y. Song, P. Zhang, S. Wang, T. hu, S. Jin, E. Lu, X. Cao, B. Wang, The influence of rhenium addition on the distribution of vacancy-type defects in tungsten, J. Nucl. Mater. in press.
[53] Xudong An, Te Zhu, Mingpan Wan, Yuanhui Li, Qianqian Wang, Peng Zhang, Jinyang Liu, Yamin Song, Zhaokuan Zhang, Baoyi Wang, Xingzhong Cao, Investigation of the interaction between hydrogen and irradiation defects in titanium by using positron annihilation spectroscopy, Int. J. Hydrogen Energ. 46 (24) (2021) 13162–13170.
[54] T. Toyama, K. Ami, K. Inoue, Y. Nagai, K. Sato, Q. Xu, Y. Hatano, Deuterium trapping at vacancy clusters in electron/neutron-irradiated tungsten studied by positron annihilation spectroscopy, J. Nucl. Mater. 499 (2018) 464–470, https://doi.org/10.1016/j.jnucmat.2017.11.022.